

# **CELLULAR MECHANOSENSING AT A DISTANCE**

**A Thesis Submitted to  
The Graduate School of Engineering and Sciences of  
İzmir Institute of Technology  
in Partial Fulfillment of the Requirements for the Degree of**

**MASTER OF SCIENCE**

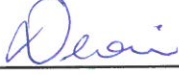
**in Biotechnology and Bioengineering**

**by  
Ali CAN**

**July 2019  
İZMİR**

We approve the thesis of Ali CAN

**Examining Committee Members:**



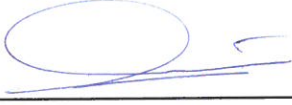
**Prof. Dr. Devrim PESEN OKVUR**

Department of Molecular Biology and Genetic, İzmir Institute of Technology



**Asst. Prof. Dr. Çiğdem TOSUN**

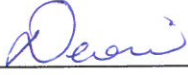
Department of Molecular Biology and Genetic, İzmir Institute of Technology



**Assoc. Prof. Dr. Şerif ŞENTÜRK**

Department of Genome Science and Molecular Biotechnology & İzmir International Biomedicine and Genome Institute, Dokuz Eylül University

17 July 2019



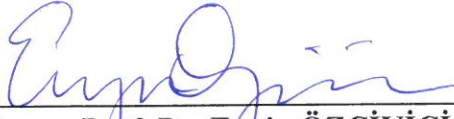
**Prof. Dr. Devrim PESEN OKVUR**

Supervisor, Department of Molecular Biology and Genetic



**Assoc. Prof. Dr. Engin ÖZÇİVİCİ**

Co-Supervisor, Department of Biotechnology and Bioengineering



**Assoc. Prof. Dr. Engin ÖZÇİVİCİ**

Head of the Department of Biotechnology Bioengineering

**Prof. Dr. Aysun SOFUOĞLU**

Dean of the Graduated School of Engineering and Science

## ACKNOWLEDGMENTS

I would like to express my gratitude to all those who gave me the possibility to complete this thesis. Firstly, I would like to express my deepest appreciation and thanks to supervisor Assoc. Prof. Dr. Devrim PESEN OKVUR for her patience, encouragement, understanding, instructive guidance and excellent support throughout this study. And also I would like to thank to my co-advisor Prof. Dr. Engin ÖZÇİVİCİ for his help and advices during analysis of the research data.

I would like to thank also the members of my thesis defense committee Assoc. Prof. Dr. Çiğdem TOSUN and Assoc. Prof. Dr. Yavuz OKTAY for helpful comments and giving suggestions.

I am greatly indebted to my colleague, and roommate Ali YETGİN for his friendship, understanding, encourages and support during the past nine years.

As teamwork is essential, I am very thankful to the members of the Controlled *in vitro* Microenvironments (CivM) laboratory for their team spirit and support.

For financial support, I would like to thank to GEBIP program and for their encouragement for science

Finally, I cannot find better words to explain my family contribution to my education and explain their love and express my thanks for their helps.

# ABSTRACT

## CELLULAR MECHANOSENSING AT A DISTANCE

The goal of the project is to determine differences in mechanical sensing at a distance between breast cancer cells and normal mammary epithelial cells. To achieve this goal, we aim to:

1. Optimize the device for mechanical sensing at a distance
2. Determine the effect of mechanical sensing at a distance on cell proliferation
3. Determine the effect of mechanical sensing at a distance on cell migration

Breast cancer is one of the cancers with the highest incidence and mortality rates in women in Turkey as well as in the world. Tumor microenvironment comprises of cancer and normal cells, extracellular matrix, soluble biological and chemical factors. Biochemical aspects of the interactions of cancer cells with the constituents of the microenvironment are widely studied whereas biophysical studies are at limited numbers.

There is increasing evidence that extracellular matrix can change the mechanics and function of cancer and stroma cells. It has been observed that cancer cells show different responses to soft and stiff tissues they are in direct contact with than normal cells. However, it is not known whether the distance at which cancer cells can feel the stiffness of a distant tissue is longer, the same or shorter than that of normal cells. The hypothesis we will test in this project is as follows: The distance at which cancer cells can feel the stiffness of a distant tissue is shorter than that of normal cells.

# ÖZET

## UZAKTAN HÜCRESEL MEKANİK ALGILAMA

Projenin amacı, meme kanseri hücreleri ile normal meme epitel hücrelerinin uzaktan mekanik algılamalarındaki farklılıkları belirlemektir. Bu amaca ulaşmak için hedeflerimiz şunlardır:

1. Uzaktan mekanik algılama aygıtının en uygun şeklinin belirlenmesi
2. Uzaktan mekanik algılama aygıtında uzaktan mekanik algılamanın hücre çoğalmasına etkisinin belirlenmesi
3. Uzaktan mekanik algılama aygıtında uzaktan mekanik algılamanın hücre göçüne etkisinin belirlenmesi

Meme kanseri dünyada olduğu gibi dünyada ve Türkiye’de de kadınlarda en sık görülen ve ölüm oranı en yüksek olan kanser çeşitlerindedir. Tümör mikroçevresi, sağlıklı ve kanserli hücreleri, hücre dışı matriksi, çözünür halde biyolojik ve faktörlerini ve kimyasal etkenleri içerir. Kanser hücrelerinin mikroçevre bileşenleri ile etkileşimlerinin biyokimyasal yönleri yaygın olarak incelenmektedir; fakat biyofiziksel çalışmalar sınırlı sayıdadır.

Hücre dışı matriksin kanser ve destek doku hücrelerinin mekaniğini ve işlevlerini değiştirebildiğine dair kanıtlar artmaktadır. Kanser hücrelerinin doğrudan temas halinde oldukları sert ve yumuşak dokulara normal hücrelerden farklı tepkiler verebildikleri de görülmüştür. Fakat kanser hücrelerinin doğrudan temas halinde bulunmadıkları dokuların sertliklerini hissedebildikleri uzaklığın normal hücrelerinkinden daha büyük, küçük veya eşit olup olmadığı bilinmemektedir. Bu uzaklığın metastaz avantajı sağlaması açısından kanser hücreleri için daha büyük olması beklenmektedir. Bu projede test edeceğimiz hipotez şu şekildedir: Kanser hücrelerinin doğrudan temas halinde bulunmadıkları dokuların sertliklerini hissedebildikleri uzaklık normal hücrelerinkinden daha uzundur.

*To my family...*

# TABLE OF CONTENTS

LIST OF FIGURES .....	v
LIST OF TABLES .....	vii
CHAPTER 1. INTRODUCTION .....	1
1.1. Microfluidic Devices .....	1
1.2. Microfluidic Devices Fabrication .....	1
1.3. 3D Printing .....	2
1.4. Photolithography .....	2
1.5. Soft-lithography .....	3
1.6. Cancer .....	4
1.7. Breast Cancer .....	5
1.8. ECM (Extracellular Matrix) and Cancer .....	5
CHAPTER 2. EXPERIMENTAL.....	8
2.1. Cell Culture .....	8
2.2. Design and Fabrication of LOC Mold .....	8
2.3. Fabrication of Lab on a Chip (LOC) .....	9
2.4. LOC Modification.....	9
2.5. Cell Tracking .....	10
2.6. Collagen Preparation.....	10
2.7. Cell Loading .....	10
2.8. Cell Viability.....	11
2.9. Collagen Permeability.....	11
2.10. Maintaining Experiment .....	13
2.11. Image Analysis Steps.....	14
CHAPTER 3. RESULTS AND DISCUSSION.....	19
CHAPTER 4. CONCLUSION .....	28
REFERENCES.....	40

# LIST OF FIGURES

<b><u>Figure</u></b>	<b><u>Page</u></b>
Figure 1.1. The photolithography steps. ....	3
Figure 1.2. Illustrative protocol for microfluidic device's fabrication by replica molding .....	4
Figure 1.3. Protrusion region and direction reprogramming in mechanic way .....	6
Figure 1.4. Growing, morphogenesis, and integrin attachments can be regulated by rigidity of matrix .....	6
Figure 1.5. The stiffness or elasticity of various epithelial tissues is compared with the elasticity of materials typically employed in tissue culture .....	7
Figure 2.1. Design and fabrication of cellular mechanosensing device at a distance .....	11
Figure 2.2. Loadings in mechanosensing at a distance device .....	12
Figure 2.3. Last version of LOC designed for cellular mechanosensing at a distance that can be seen in different angles .....	12
Figure 2.4. Illustrative scheme for depicting expected results. ....	13
Figure 2.5. Microscope image was opened in Zeiss application. ....	14
Figure 2.6. Fluorescence channel in the image was separated from the image and saved. ....	14
Figure 2.7. Obtained single channeled fluorescence image's Z-stack images were saved separately. ....	15
Figure 2.8. Color split macro in ImageJ .....	15
Figure 2.9. Sum macro in Image J .....	16
Figure 2.10. Sum Image.....	16
Figure 2.11. LOC's interface was emphasized with a line, and the image was rotated in the manner of the line's angle become zero .....	17
Figure 2.12. The background was subtracted from angle fixed image.....	17
Figure 2.13. Three different zones with same size ROI (region of interest) were determined .....	17
Figure 2.14. Then, the image was transformed to black and white pixel including images with threshold tool in ImageJ .....	18
Figure 3.1. Collagen Detachment from PDMS without surface modification .....	19
Figure 3.2. The image of normal cells inside LOC. Whole LOC image and zoomed in image of a region.....	20



<b><u>Figure</u></b>	<b><u>Page</u></b>
Figure 3.3. Cancer cells' image inside LOC.....	20
Figure 3.4. Illustrative scheme for obtained results.....	21
Figure 3.5. Quantitative analysis of cellular migration .....	21
Figure 3.6. Sum of pixels in the regions where cells were found ANOVA $p < 0.11$ .....	22
Figure 3.7. Sum of migrated distance for each region ANOVA $p < 0.002$ and $P \leq 0.001$ among each region.....	22
Figure 3.8. Average migrated distances for each region ANOVA $p < 0.005$ .....	23
Figure 3.9. Linear Regression Analysis for Mean Distance, Tension and Max Distance Anova $p < 0.005$ .....	23
Figure 3.10. Illustration of migrated and remained distance .....	24
Figure 3.11. Tension for each zone, ANOVA $p < 9.3 \times 10^{-6}$ .....	24
Figure 3.12. One site-Fit Curve logIC50 for tension.....	25
Figure 3.13. Critical Distance Point on LOC, $450 \pm 7.1 \mu$ .....	25
Figure 3.14. Collagen Detached from PDMS (After 6 days) .....	25
Figure 3.15. Death Index value(Viability) comparison among three zones, ANOVA $p < 0.5978$ .....	26
Figure 3.16. Permeability comparison among three zones, ANOVA $p < 0.3988$ for t1 and ANOVA $p < 0.1264$ for t4 .....	27

# LIST OF TABLES

<b><u>Table</u></b>	<b><u>Page</u></b>
Table.1. Correlations between different parameters .....	26

# CHAPTER 1

## INTRODUCTION

### 1.1. Microfluidic Devices

Microfluidic devices are used widely for scientific reasons. Small sizes of these devices make them advantageous in cost for manufacturing and experiments, time for analysis, harmful waste product production, and transportability. Additionally, these devices make it easier for studies which are difficult to do in large devices. For instance, microfluidic channels have appreciate size and circumstances for flow present *in vivo* in capillaries [1]; usage of these microfluidic devices with similar size and elasticity found in nature results in precise info and better understand of physiology. Besides, resolution is increased while device's size is decreased, however smaller channels lead detecting to become more difficult and easy to become blocked by particles [2].

Traditional devices and methods can only be used for averaged measuring and difficult for usage in analyzing of dynamic techniques for multicellular researches and lack of productivity. Briefly, they are not useful for getting accurate mechanistic perspective [3].

### 1.2. Microfluidic Devices Fabrication

First example of microfluidic device fabricated at Stanford University was miniaturized GC in 1970s. Microfluidic devices which are used for fluidic solutions were evolved in four laboratories; Manz, Harrison, Ramse, and Mathies. Fabrication of these devices was done with current developed technology in those years by microelectronics and photolithography and etching was done in silicon/glass[4]. In addition to these techniques, 3D printing is another current technique for fabrication of molds from resin with less cost and faster improved resolution. Additionally, 3D printing takes less time than photolithography for the fabrication of the mold. In photolithography all process is done almost for 3 days, however some hours in 3D Printing.

### **1.3. 3D Printing**

3D-printing has recently attracted attention as a way to fabricate microfluidic systems due to its automated, assembly-free 3D fabrication, rapidly decreasing costs, and fast-improving resolution and throughput. 3D-Printing is a rapid-prototyping, 3D digital manufacturing process that affords production of small batches of parts while allowing for a smooth transition to injection-molding for those applications that demand high-throughput production. “3D-printing” refers to a set of additive manufacturing techniques, which can create solid three-dimensional (3D) objects layer-by-layer under precise digital control. Of these techniques, the ones that are most relevant to microfluidic device fabrication are (a) stereolithography (SL), (b) multi jet modeling (MJM) and (c) fused deposition modeling (FDM) [5].

### **1.4. Photolithography**

Photolithography is the technique in which shapes/figures on mask transposed on the sample by UV. Masks are manufactured from quartz base which is covered with chromium that is non-transparent with wanted geometric shapes. These designs/shapes on masks can be produced with the help of AutoCAD software and then can be produced in clean room by the designer or can be manufactured in companies. These masks can have down to 1mm resolution [6].

Normally photolithography was developed for manufacturing of the semiconductor systems. Silicon wafer is commonly utilized as substrate matter that has good semi-conductor properties and is flat in atomic level. Transparent wafers such as quartz and glass can be used in biological researches and more appropriate in optical microscopy. UV-sensitive substrate called photoresist (PR), needed for transfer of the patterns onto sample from mask. After coated with PR, the wafer is baked on heater. Then the mask and wafer are brought into close contact (gap between wafer and mask I changeable). Afterwards, the latter with UV source is putted on the mask protected wafer. For positive PR, irradiated areas turns to soluble phase and can be removed by development protocol. These steps in the process are summed up in Fig.1.1. On the other hand, in negative PRs, irradiated areas turn to insoluble phase, by this way

negative image is generated in regard to the. In the development process, patterned surface is able to become removed with chemicals [6].

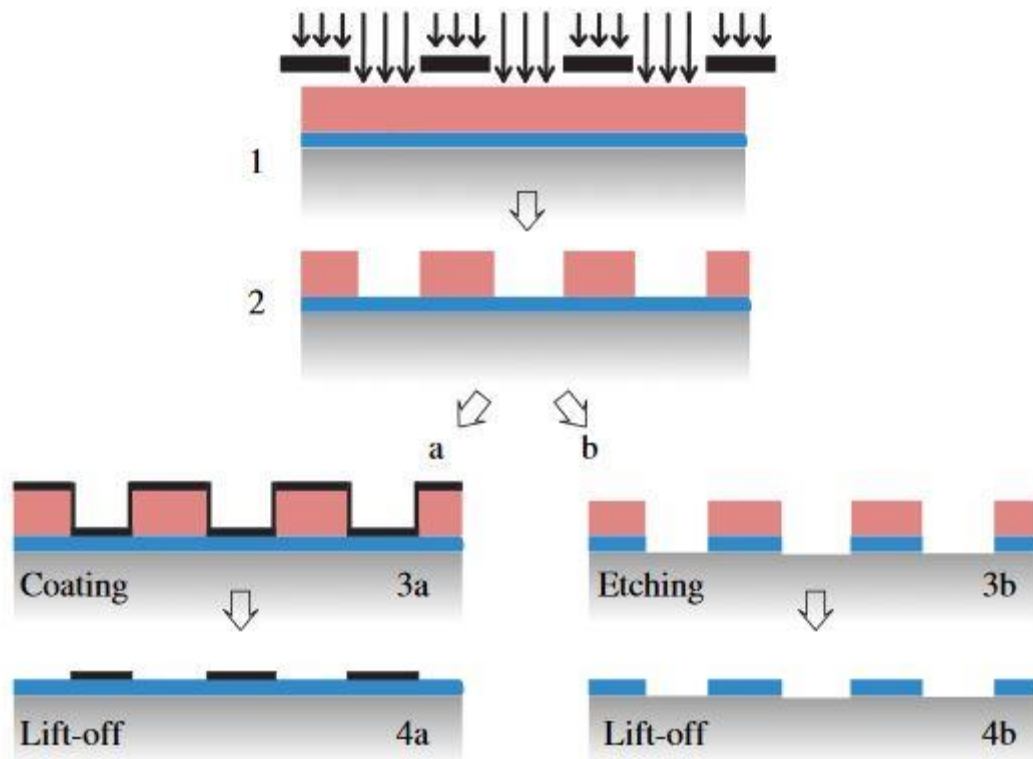


Figure 1.1. The photolithography steps. 1. UV exposing to a coated photoresist (PR) on a mask; 2. Development of PR to make underlying substrate locally accessible. Then two different routes are followed. Route a: Deposition (3a.) with metal or biological molecules (proteins, peptides and etc.) and lifting-off process by solvent (4a). Route 3b: use of patterned PR as a new mask to dry etches of metal-oxide layer 4b lifting-off process for remained PR(Source: Falconnet, D., et al. [6] ).

### 1.5. Soft-lithography

One of the other microfabrication techniques is soft lithography in which elastomeric stamps are used for doing print and mold of pattern. For biological purposes, soft lithography has pluses in compared to photolithography. Particularly, surfaces' molecular structure can be controlled and biology relevant complex molecules can be patterned and for fabrication of microfluidic suitable channel structures and also

for patterning and manipulating cells. Besides, systems with larger size in biology i.e., greater than or equal to  $50\mu\text{m}$  producing the prototype structures/patterns is not expensive, rapid and convenient [7].

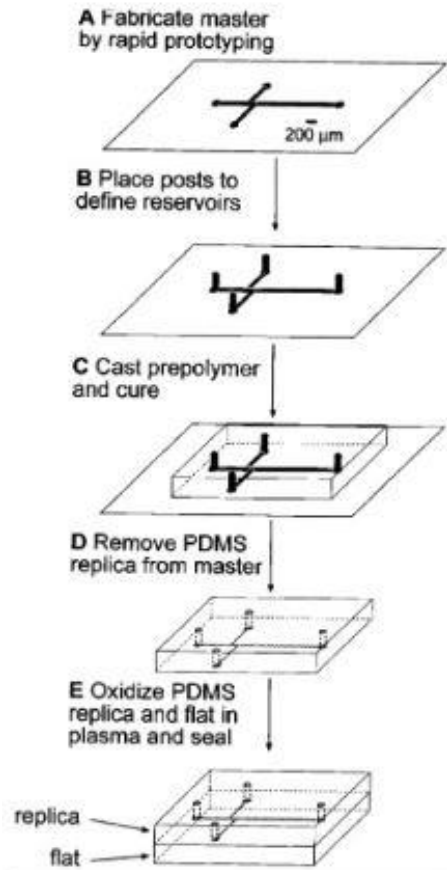


Figure 1.2. Illustrative protocol for microfluidic device's fabrication by replica molding. A: fabrication of the master with the method of rapid prototyping, B: Post formation for defining of reservoirs, C: Polymer(PDMS) casting and curing D: Removing of polymerized PDMS from master/mold E: Bonding of the PDMS after oxidization on glass (Source: McDonald, J.C., et al. [4]).

## 1.6. Cancer

Normal cells can be transformed into cells (cancer) which have imbalance in growth regulation that leads to uncontrolled proliferating of them after some genetic changes[8]. Cancer ranks the first place as death reason in developed countries and ranks the second place in developing countries. In developing countries, aging, growth

of population and also cancer leading lifestyle preferences such as smoking, less physical activity and unhealthy diets [9].

## **1.7. Breast Cancer**

Breast cancer is the type of cancer where the cells in breast tissue transform into cancer cells and it is the main reason of death among women in whole world. In the world breast cancer is accountable for more than estimated one million neoplasms among 10 million neoplasms globally each year for both of the sexes[10]. Additionally, it is the major cause of cancer reasoned death among women worldwide and in 2000 375,000 deaths happened [11].

## **1.8. ECM (Extracellular Matrix) and Cancer**

Extracellular matrix (ECM) is 3D macromolecular structure that formed from many different molecules such as collagen, elastin, laminin, some other glycoproteins and fibronectin[12]. Fibers inside ECM can be aligned and concentrated in mechanic way by cells and multicellular structures and also they are able to sense and react to mechanical effectors by differentiation, branching and disorganization.

The ECM help tissues for the formation of mechanical integrity in structure and also supplies chemical, anatomic and mechanic signals for cells and by this way affects them in differentiating, developing and pathogenesis [13].

Microenvironment of cancer cells has significant roles in cancer cells' development. Deregulations and disorganizations occur in ECM during diseases (for example cancer), although it's controlling is tight during homeostasis of organ and developing of embryo. Transformed ECM has roles for cancer progressing by encouraging cancer cells to transforming and metastasis after disease occurrence. Significantly, stromal cells are also affected from the anomalies in ECM by facilitating tumor associated angiogenesis and occurrence of inflammation. Therefore, stromal cells also play important role in the formation of tumor microenvironment [14].

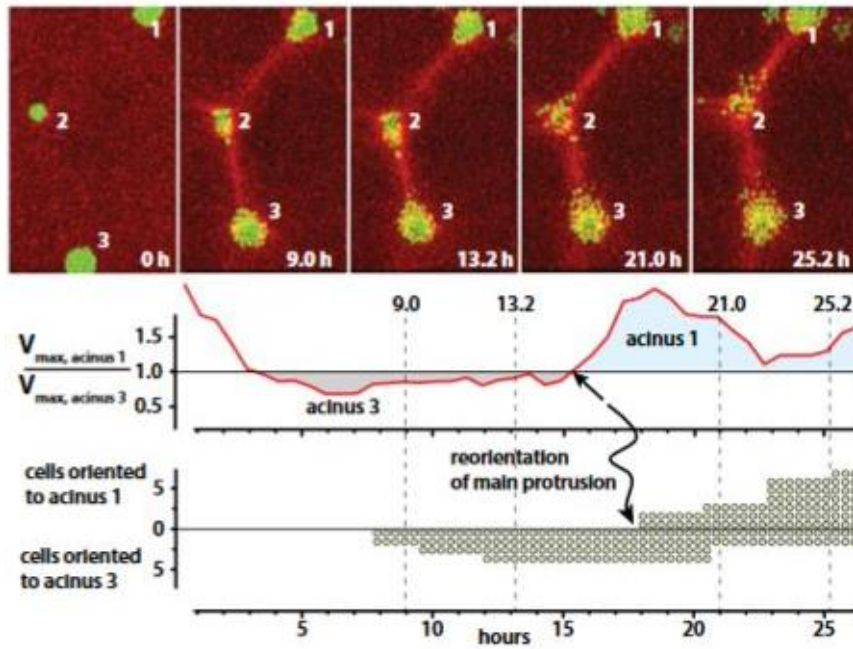


Figure 1.3. Protrusion region and direction reprogramming in mechanic way (Source: Shi, Q., et al. [13]).

At first, acinus 3 pulls collagen quickly, and cells start leaving acinus 2 towards acinus 3 at  $t=7$  h. Then at  $t=15$  h, acinus 1 starts to pull quicker than acinus 3 [13].

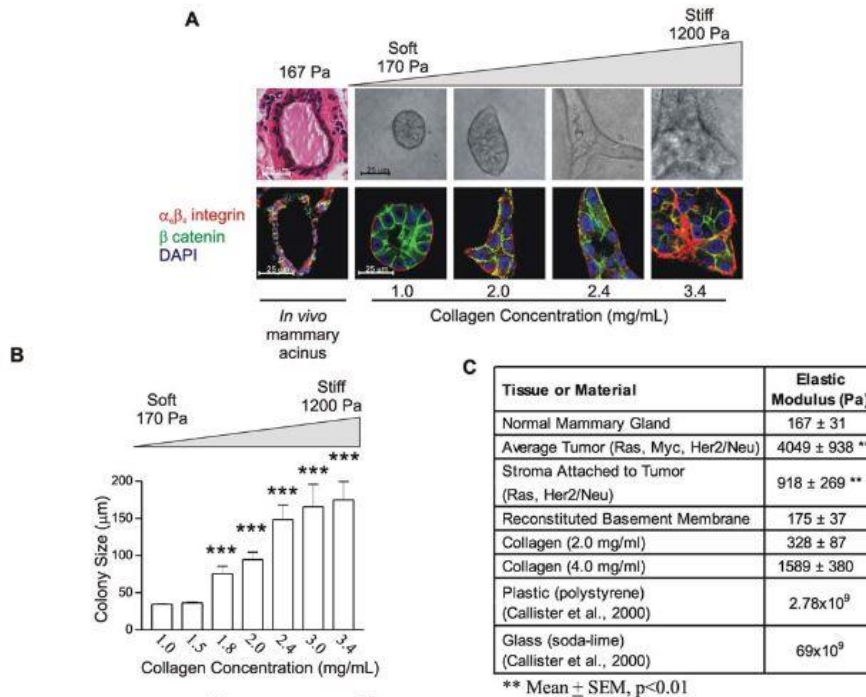


Figure 1.4. Growing, morphogenesis, and integrin attachments can be regulated by rigidity of matrix (Source: Paszek, M.J., et al. [15]).



In figure 1.4 A part top right: phase images and H&E-stained tissue illustrating normal morphology of the mammary gland duct in a compliant gland (167 Pa), in contrast to MEC colonies which were grown in BM/COL I gels of raising stiffness (170–1200 Pa). Bottom: confocal immunofluorescence (IF) images of tissue section of a mammary duct and cryo-sections of MEC colonies which were grown as above, stained for  $\beta$ -catenin (green),  $\alpha$ 6 or  $\beta$ 4 integrin (red), and nuclei (blue). B: Colony size of MECs which were grown as shown in A. \*\*\*p%0.001. C: Elastic modulus of normal mouse mammary gland and formed tumors from MMTV-Her2/neu, Myc, and Ras-transgenic mice; normal value for tumor-adjacent stroma, in contrast to BM and COL gels; and regular glass and polystyrene substances utilized for monolayer culture. Values show the mean  $\pm$  SEM of four measuring from multiple mice and gels. \*\*p%0.01 [15].

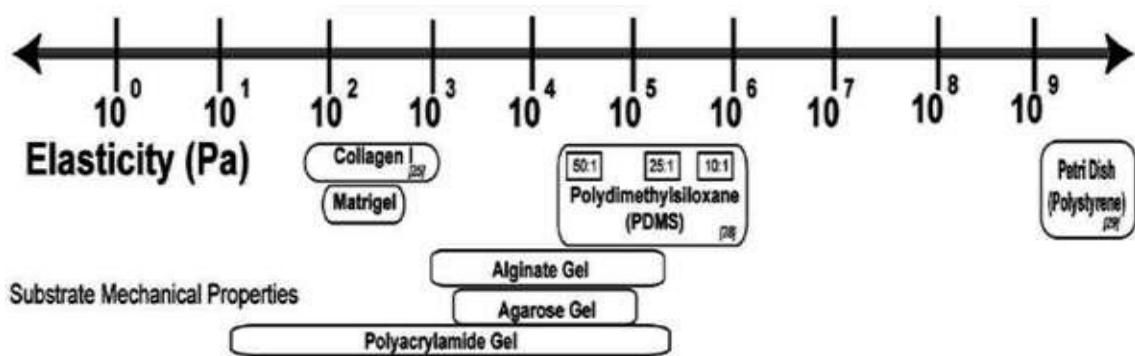


Figure 1.5. The stiffness or elasticity of various epithelial tissues is compared with the elasticity of materials typically employed in tissue culture (Source: Kolahi, K.S., et al. [16]).

## **CHAPTER 2**

### **EXPERIMENTAL**

#### **2.1. Cell Culture**

In the experiments, two types of cell lines were used; MDA-MB-231 cancer cells and MCF-10A epithelial cells. These cell lines were grown in petri dishes and their passaging was done when the petri dish became confluent. Each cell line has their specific gradients of medium. For MDA-MB-231; 450ml DMEM (Dulbecco's Modified Eagle Medium), 50ml FBS (Fetal Bovine Serum), 5ml L-glutamin, and 5ml Pen-Strep were used. For MCF-10A; 500ml DMEM-F12, 25ml Donor Horse Serum, 100ul EGF(Epidermal Growth Factor), 250ul Hydrocortisone, 50ul 100ng/ml Cholera toxin, 500ul 10ug/ml Insulin, 5ml Pen-Strep( 1X 100U pen + 100ug/ml strep fc) and 5ml L-glutamin (2mM fc, 200mMsc). For cell culture passaging, after petri dishes become confluent, old medium was removed from petri and then Trypsin EDTA Solution C (0.05%), EDTA (0.02%) was added for removing floating dead cells. Then Trypsin was used again for removing the cells from petri dish, but for removing Trypsin was incubated for enough time till cells detach from the petri. After incubation, cell's own medium added to neutralize the Trypsin's effect and petri dish was washed with this mixture. Then, this medium, trypsin and cell mixture was collected in a falcon and centrifuge at 1000 rpm for 5min was done to get rid of supernatant and get cells. After taking out the supernatant from falcon, cell medium was added to cells and mixed, then after pipetting mixture, cells with different percentages were planted into new petri dishes with fresh medium.

#### **2.2. Design and Fabrication of LOC Mold**

The design of the LOC device was done with AutoCAD application on computer. After design of the LOC completed, it was used for fabrication with 3D printer from resin.

### **2.3. Fabrication of Lab on a Chip (LOC)**

For fabrication of LOC devices we firstly need molds (patterns), for my thesis 3D printer was used but in conventional method UV-lithography was another option for molds. After printing of mold was done, they were ready for fabrication of LOC devices. These devices were fabricated with use of PDMS (Polydimethylsiloxane). PDMS was mixed with curing agent in 10:1 ratio, and then mixing was done till we get white color with many bubbles. After that, this PDMS mixture was vacuumed to get rid of bubbles. Then this mixture was poured on molds which were washed before and vacuum was done again for removing bubbles. For polymerization, they were incubated at 60 °C for 16 hours.

After polymerization was done, PDMS was removed from molds and I made holes and cut the extra parts of PDMS. With the use of alcohol and water, PDMSs were washed in sonicator. After washing, PDMSs were waited for drying for 24 hour at room temperature to get ready for bonding on glass with UV-Ozone device. Ozone in the device make the glass and PDMS surfaces ready for binding each other, and UV help to get rid of contaminant on both of the glass and PDMS. Glass and PDMS that will be attached to each other were putted into UV-Ozone device and machine was turned on for 5min. After this time, PDMS and glass were bonded each other. Then, bonded LOC was incubated on 100°C heater for 15min. After completing incubation; LOCs were incubated under UV light for sterilization and at 80°C for 24 hours for stabilization of the bonds between PDMS and glass.

### **2.4. LOC Modification**

LOC modification was done with (3-Aminopropyl)-triethoxysilane (APTES). For APTES modification; LOCs were loaded with %2 APTES in acetone solution. Then, LOCs incubated for 15min, then washed three times with PBS and three times with upH2O. LOCs were ready for binding of collagen to free NH<sub>2</sub> ends of APTES, use no need of incubation of LOCs at 80°C after bonding step. After APTES modification of LOCs, they were stayed inside vacuum box to prevent contamination and deformation of APTES inside LOC at room temperature.

## **2.5. Cell Tracking**

In the experiments two different cell lines were used; MDA-MB-231 and MCF-10A. Firstly both of the cell lines tracked with green tracker (GFP). But then, dsRed infected MDA-MB-231 cell lines were used but keep tracking MCF-10A.

## **2.6. Collagen Preparation**

In the experiments, 3mg/ml collagen was used after diluting it from 9.66 mg/ml collagen solution. The ingredients required for collagen polymerizations were; NaOH, DMEM, H<sub>2</sub>O and collagen. For NaOH amount for the mix was calculated with multiplying collagen amount with 0.23, for DMEM; 1:10 of total mix. Rest of the mix was filled with H<sub>2</sub>O. Collagen was added lastly to this mix, and then collagen mix was loaded into LOCs immediately and incubated for 30min. For prevention of the drying and maintaining the moisture, 10ml of H<sub>2</sub>O was added into LOCs' container.

## **2.7. Cell Loading**

For cell number optimization,  $10^5$ ,  $10^6$ , and  $2 \times 10^5$  cells/ml were tried and it was observed that  $10^6$  was better number of cells for observation of migration in LOCs. After collagen polymerization, calculated number of cells in cell medium was loaded on collagen and all the holes were closed with tape. Finally LOCs were placed into incubator at 37°C.

The design of the LOC (lab-on-a-chip) had been changed during thesis research. Instead of loading cells in matrix, they were loaded inside their culture medium and the design of the LOC is determined according to cells collapsing on up line of the matrix by the help of gravity effect principle. (Figure 2.1, Figure 2.2, Figure 2.3). Besides, the distance between cells and PDMS which was the material that was going to be sensed by cells was designed to be variable. (Figure 6, Figure 8). By this way, it was planned to investigate cells' reaction to different distances in a LOC.

## 2.8. Cell Viability

For measurement and analysis of cellular viability in collagen, cells were incubated with Hoechst 33342/PI (propidium iodide) Double Stain for 40min diluted in cell media. Cells emitting blue fluorescence were Hoechst positive while those with red fluorescence were PI positive. Zeiss fluorescence microscope was used for image acquisition, and analysis were done with ImageJ program.

## 2.9. Collagen Permeability

For measurement of the collagen permeability, dextran (1/200) was used after experiment completed after 2 days. Zeiss fluorescence microscope was used for image acquisition for 40min with 10min intervals.

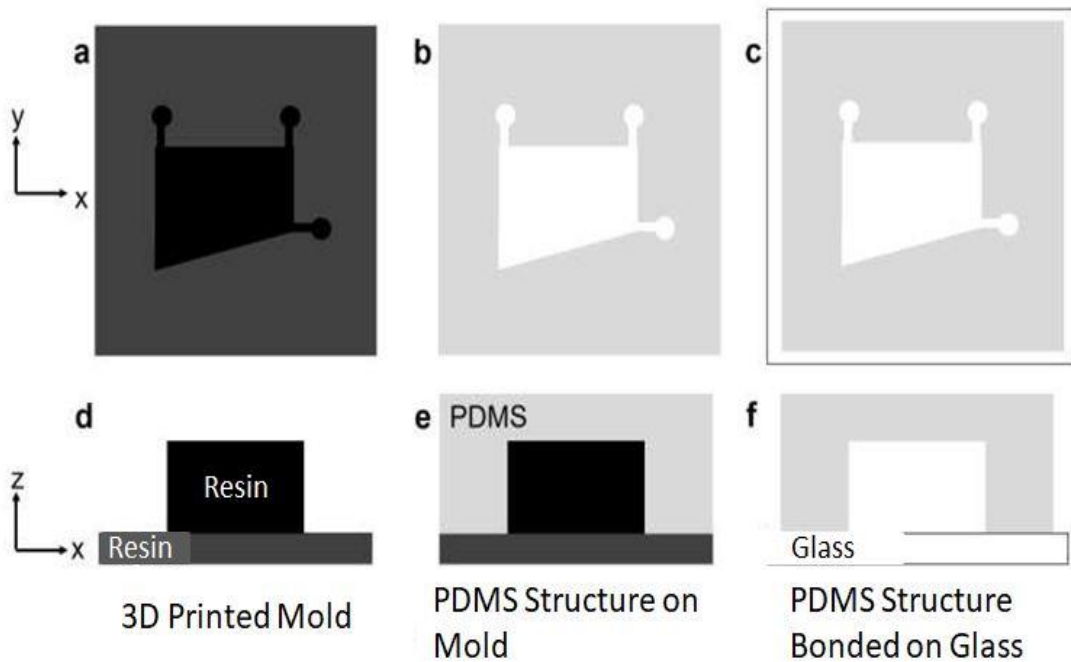


Figure 2.1. Design and fabrication of cellular mechanosensing device at a distance.

In figure 2.1 a,d. part shows Resin mold printed with 3D-Printer b,e. Polymerized PDMS structure on resin mold. c,f. Bonded PDMS structure with glass a,b,c View from above. d,e,f lateral section view. The length of PDMS structure along with x axis and y axis is variable because of mold.

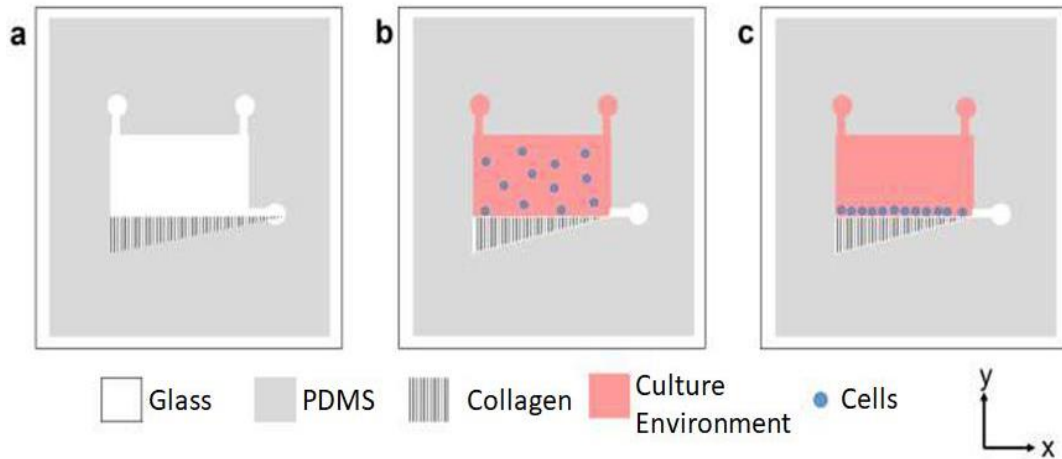


Figure 2.2. Loadings in mechanosensing at a distance device. a) Hydrogel loaded device. b) Cell loaded device in culture environment c) Collapsed cells on matrix with the gravity effect

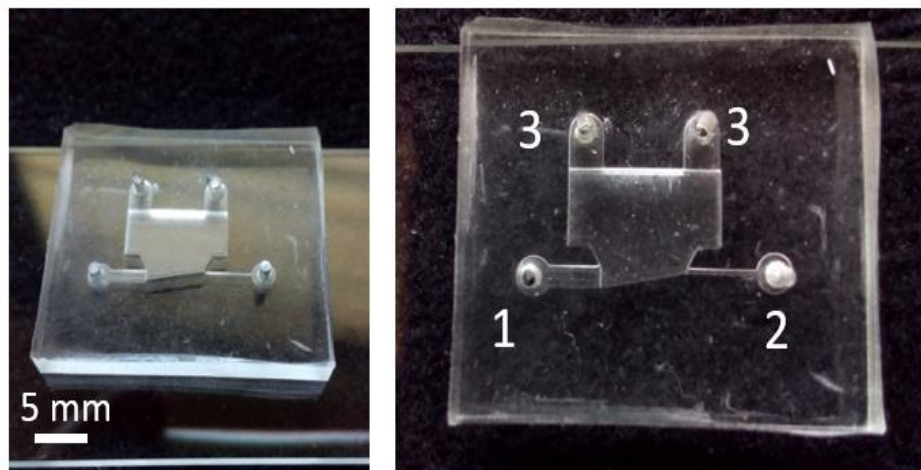


Figure 2.3. Last version of LOC designed for cellular mechanosensing at a distance that can be seen in different angles. Collagen was loaded from the hole numbered as 1, loading was completed when collagen reached to number.2, and number 3-4 were used for culture media and air entry-exist. The height of entry-exist connection channels is 0.2mm and the height of collagen and culture media regions is 1mm.

Expected results with LOC are shown in Figure 2.4. Hypothesis: The length of cancer cells' ability to sense the stiffness of a distant tissue is shorter than that of normal cells. If the hypothesis is right, the results are expected to be seen like Figure.8c.

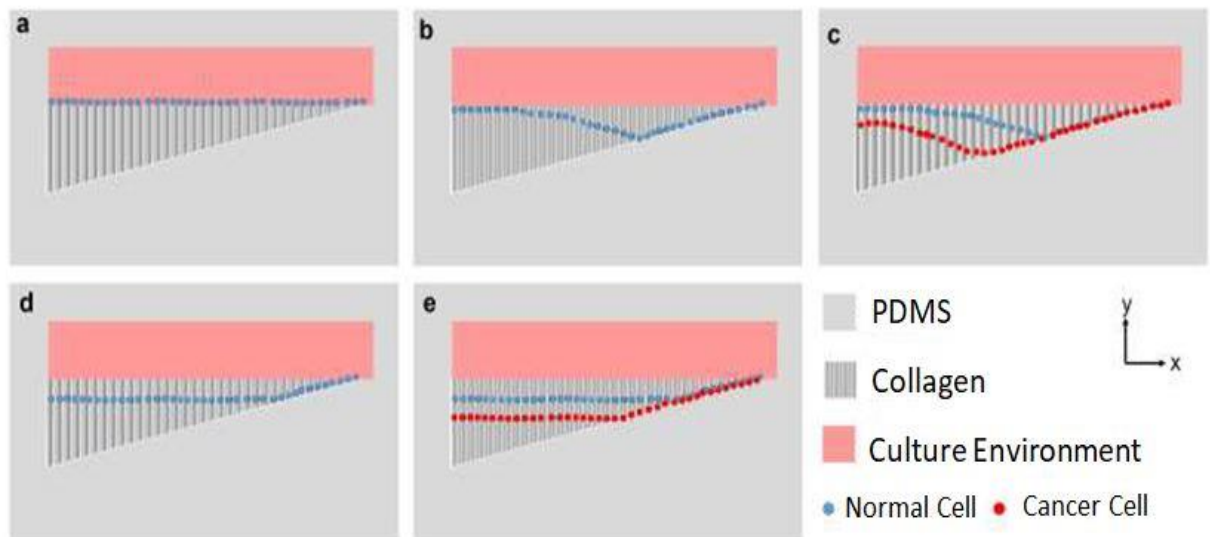


Figure 2.4. Illustrative scheme for depicting expected results.

In Figure 2.4, a. part is the side view of collapsed cells on collagen surface. b. If cells sense stiff surface better, they will show nonlinear distribution in figure c. If cancer cells sense stiff surfaces better than normal cells, their distribution will be different than normal cells and expected to become like in the figure. d. If there is no difference in mechanosensing at a distance, it is expected cells to be distributed at same distance. e. If there is no difference in mechanosensing at a distance but there are mechanosensing differences between normal and cancer cells, their distribution is expected to become like the figure. Blue dots are the normal epithelial cells (MCF-10A) and red dots are breast cancer cells (MDA-MB-231). Collagen concentration is 3mg/ml and cell concentration is  $10^6$  cell/ml and each cell was tracked with color (green or red) trackers.

## 2.10. Maintaining Experiment

After putting LOCs with 3mg/ml concentration of collagen and  $10^6$  cell/ml contraction of color tracked cells into incubator at 37°C, container's water amount almost 3-4ml and LOC's medium (50ul for each LOC) were checked every two day. Image acquisition was done with Zeiss fluorescence microscopy, and images were acquiesced for observation of cellular migration for every day.

## 2.11. Image Analysis Steps

Image analysis steps can be seen below this paragraph step by step explained with screenshots of the programs' steps.

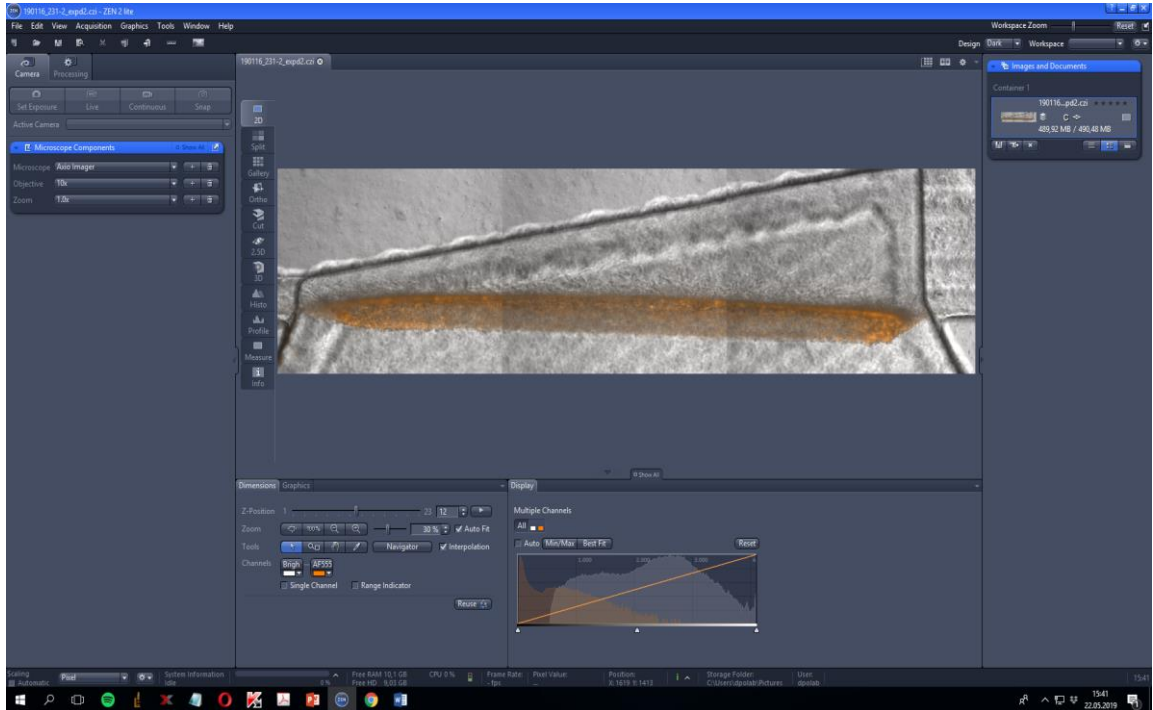


Figure 2.5. Microscope image was opened in Zeiss application.

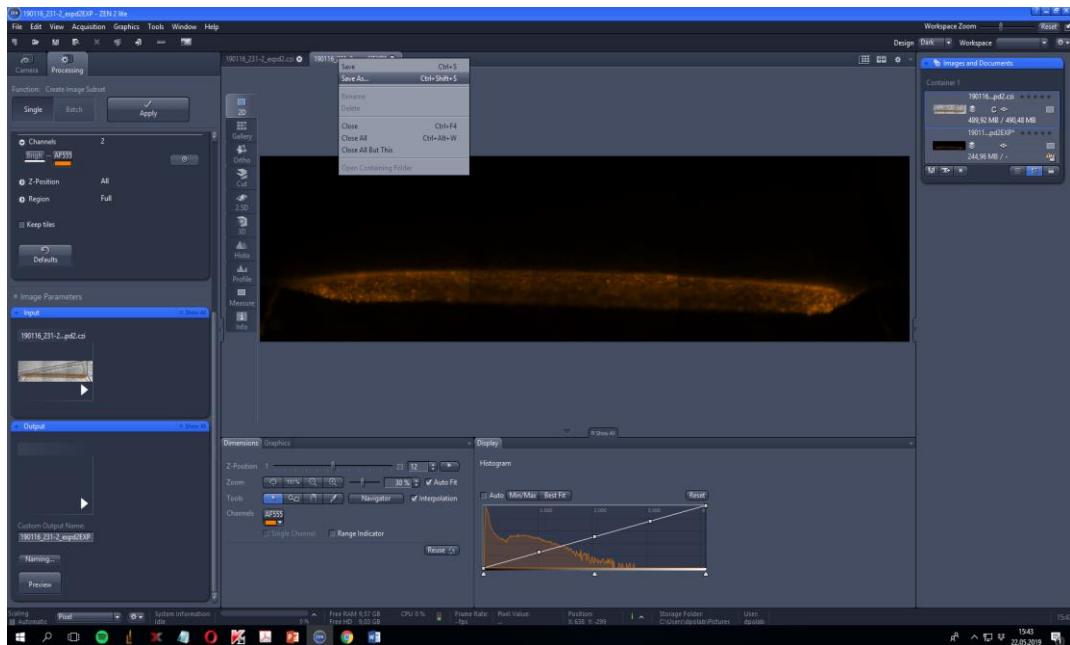


Figure 2.6. Fluorescence channel in the image was separated from the image and saved.



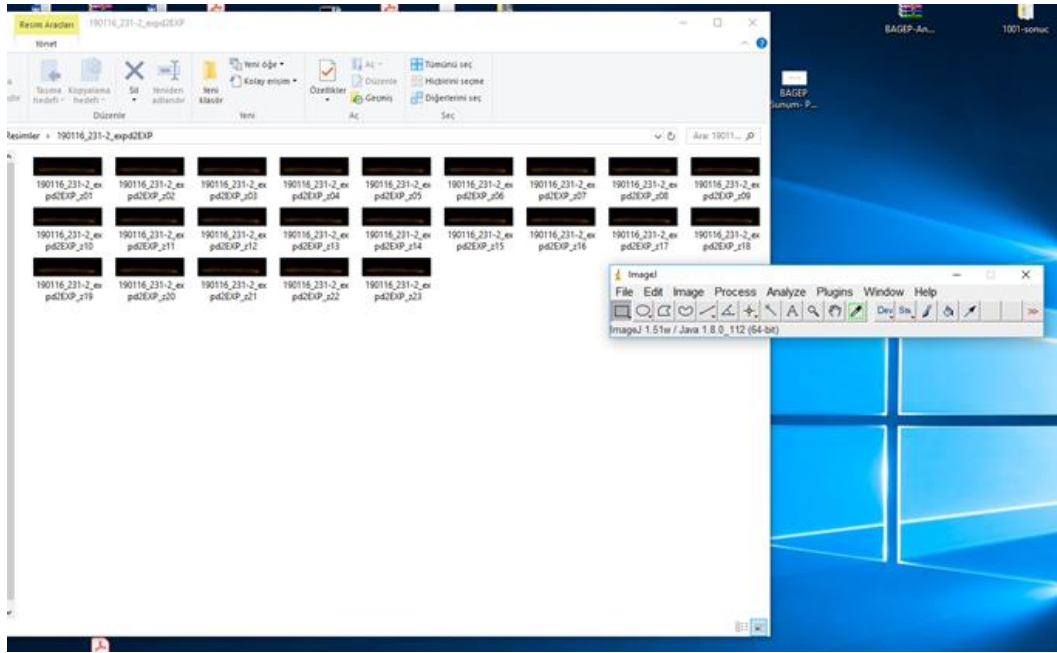


Figure 2.7. Obtained single channeled fluorescence image's Z-stack images were saved separately.

```

MacroGREENSplitjpg
File Edit Font Examples Macros Debug
macro "Batch split color16to8bit" {
    requires("1.33s");
    run("Close All");
    dir = getDirectory("Choose a Directory ");
    list = getFileList(dir);
    setBatchMode(true);
    for (i=0; i<list.length; i++) {
        path = dir+list[i];
        open(path);
        run("Split Channels");
        close();

        dotIndex = lastIndexOf(path, ".");
        if (dotIndex!=-1)
            path = substring(path, 0, dotIndex); // remove extension
        save(path+"-green.jpg");
        close();
        close();
    }
}

```

Figure 2.8. Color split macro in ImageJ.

```
SumMacroACv6
File Edit Font Examples Macros Debug
macro "Z project folder" {
  requires("1.33s");
  dir = getDirectory("Choose a Directory ");
  list = getFileList(dir);
  setBatchMode(true);
  for (i=0; i<list.length; i++) {
    path = dir+list[i];
    open(path);
  }
  run("Images to Stack", "name=Stack title=[] use");

  run("Z Project...", "projection=[Sum Slices]");

  save(path+"-Zsum.tif");

  close();
}
```

Figure 2.9. Sum macro in Image J.

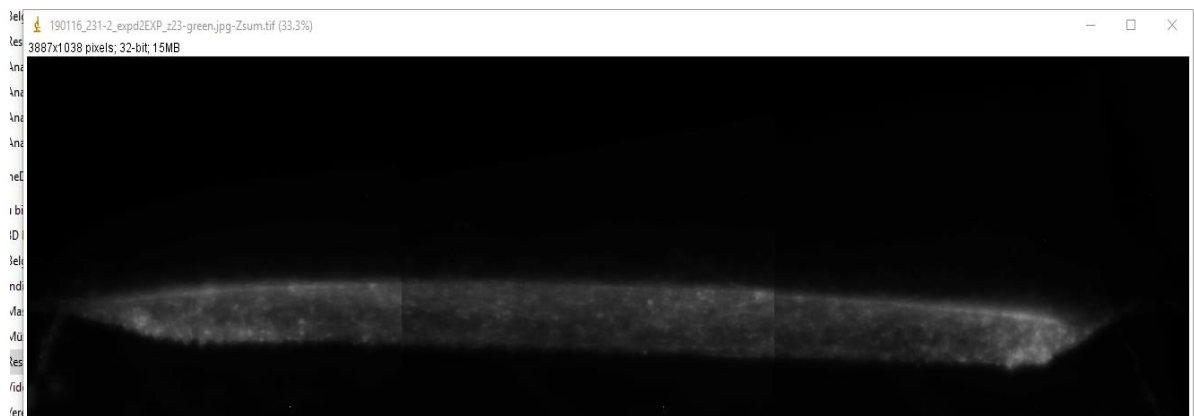


Figure 2.10. Sum Image

RGB Z-stack images were transformed to single color images with ImageJ macro (Figure 2.8) and with another ImageJ macro (Figure 2.9) sum image was obtained from Z-stack images.

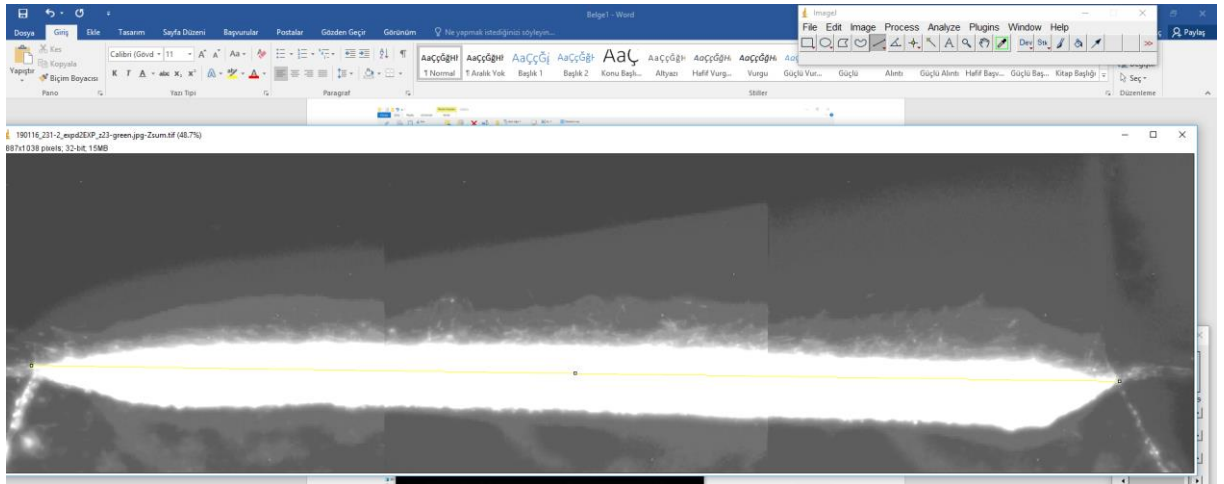


Figure 2.11. LOC's interface was emphasized with a line, and the image was rotated in the manner of the line's angle become zero (0).

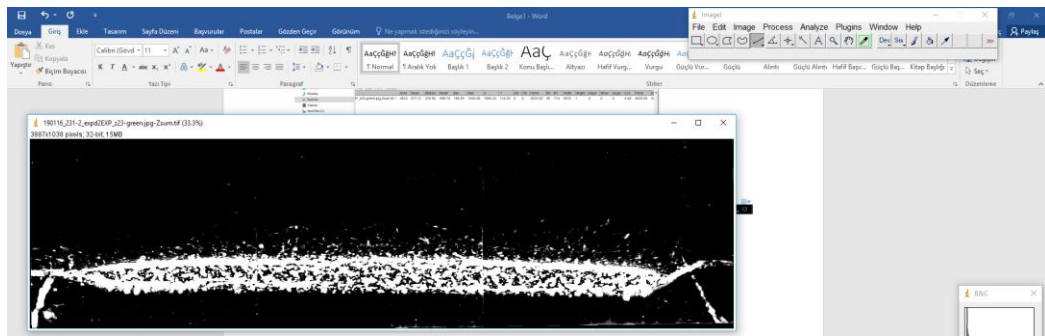


Figure 2.12. The background was subtracted from angle fixed image.

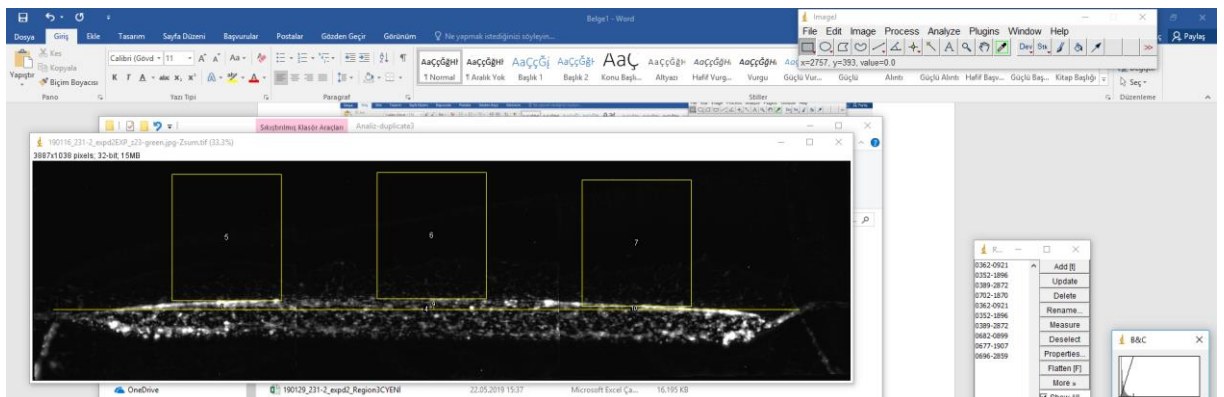


Figure 2.13. Three different zones with same size ROI (region of interest) were determined. ROIs were set to zero to beginning of collagen gel. Because the beginning of collagen gel is different than LOC interface, the distance between them was used for further calculations.

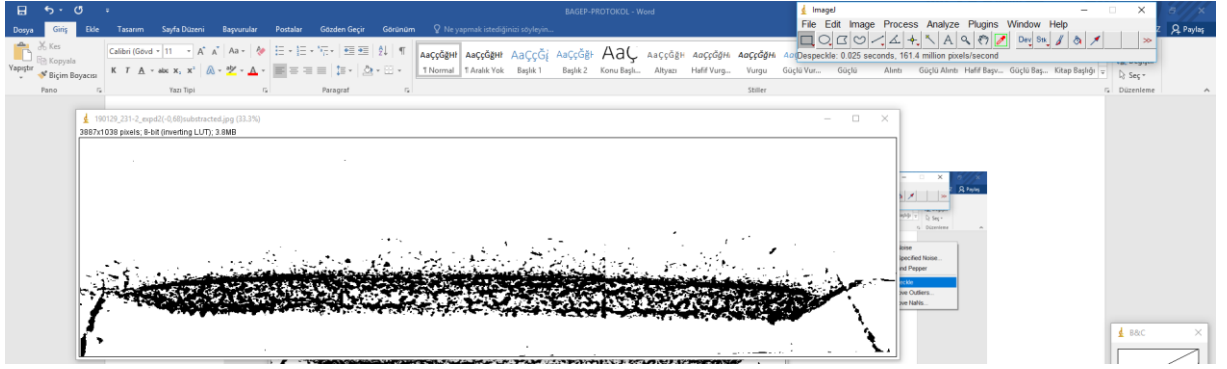


Figure 2.14. Then, the image was transformed to black and white pixel including images with threshold tool in ImageJ. Background was decreased with despeckle tool and analysis were done with this last image.

For each ROI region  $x,y$ , and intensity values were saved, and then these values transferred to excel for analysis. Distance was calculated for each bright pixel from collagen gel beginning.

## CHAPTER 3

### RESULTS AND DISCUSSION

Without surface modification collagen was not able to attach to PDMS surface as can be seen in Figure 3.1.

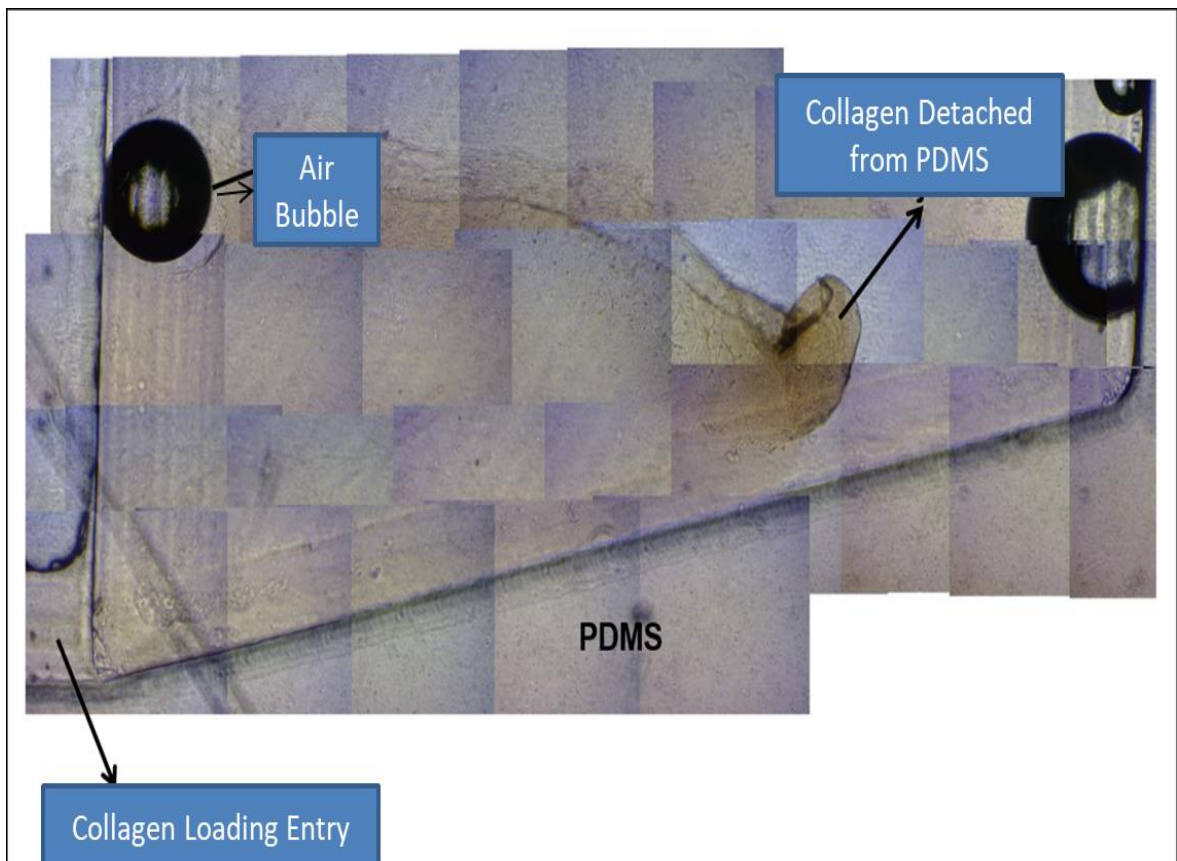


Figure 3.1. Collagen Detachment from PDMS without surface modification after 24 hours cell loading.

Normal epithelial cells (MCF10A) didn't migrate in all experiments (Figure 19). However, breast cancer cells (MDA-MB-231) migrated (Figure 20). Expected result was the increasing of migration when the distance to PDMS decreases. The assumption was based on positive feedback effect of stiff material at a distance. In contrary to expected, cellular migration increased when the distance to stiffness (PDMS) increased (Figure 21, 22). This result shows stiffness at a distance is doing negative feedback.

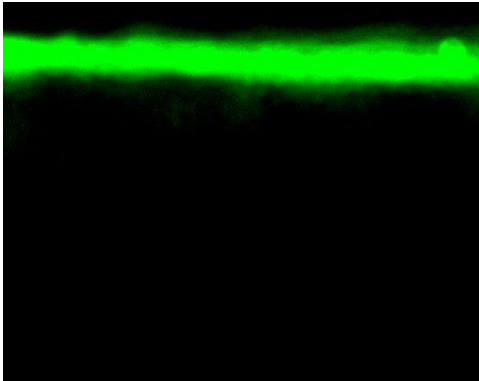
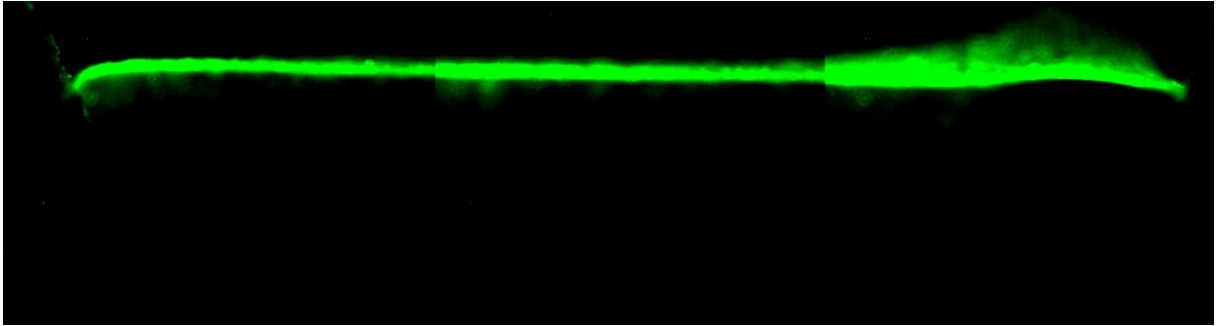


Figure 3.2. The image of normal cells inside LOC. Up: whole LOC image and down: zoomed in image of a region.

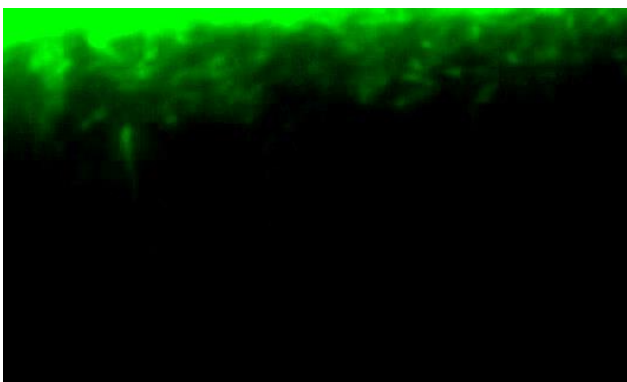
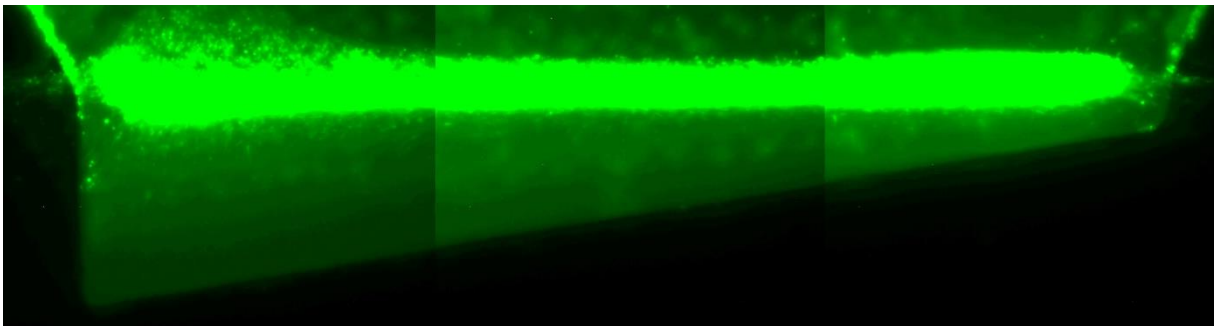


Figure 3.3. Cancer cells' image inside LOC. Up: whole LOC image and down: zoomed in image of a region.

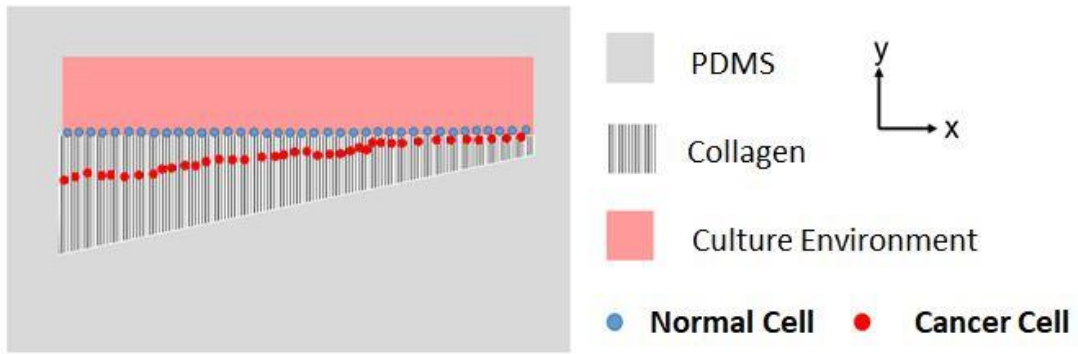


Figure 3.4. Illustrative scheme for obtained results. No migration in normal cells, the migration increased in cancer cells when the distance to PDMS increased.

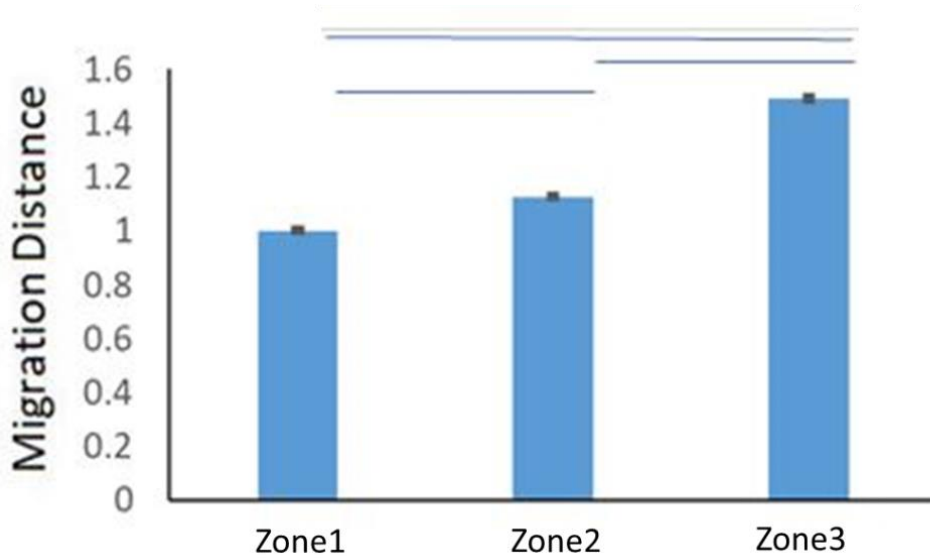


Figure 3.5. Quantitative analysis of cellular migration. Migrated distance averages are shown for 3(three) different zones. Migrated distances are normalized to 1<sup>st</sup> zone's average distance. zone 1 is the narrow part, and zone 3 is the deepest part of the LOC. Error bars show the standard errors and horizontal lines show regions which are different from each other. t-test  $p < 0.00001$ . Biological repeat number = 2-3, Technical repeat number = 2.

Total cellular area is investigated for each region. Because cells' pixel value is different than zero where cells are found, sum of these pixels are taken or determination of cellular area. Total cellular area is normalized to 1<sup>st</sup> region's cellular area (Figure 3.5). Any significant difference couldn't be found among regions.

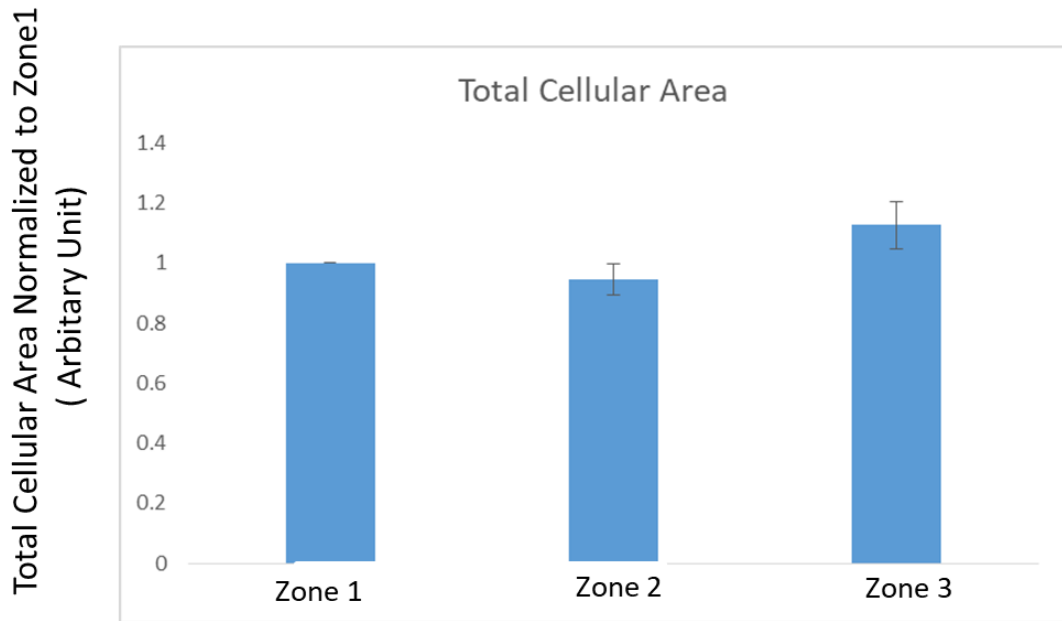


Figure 3.6. Sum of pixels in the regions where cells were found ANOVA  $p < 0.11$ .

Total migrated distance investigated for each region. 2<sup>nd</sup> and 3<sup>rd</sup> regions are normalized to 1<sup>st</sup> region data (Figure 3.6). Significant difference found between regions, and total migration distance was higher than region 1 and 2. Although total cellular area was same, migration distance was different from each other.

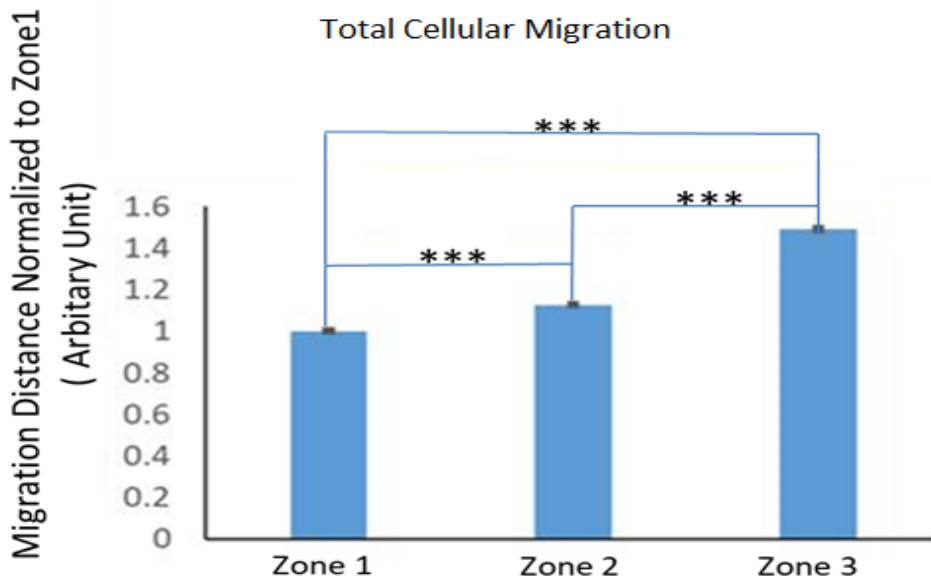


Figure 3.7. Sum of migrated distance for each region ANOVA  $p < 0.002$  and  $P \leq 0.001$  among each region.



Migrated distance average is investigated for each region, and 2<sup>nd</sup> and 3<sup>rd</sup> regions were normalized to 1<sup>st</sup> region (Figure 3.7). Significant difference was found between regions ANOVA  $p < 9.3 \times 10^{-6}$  and average migrated distance was higher in the LOC.

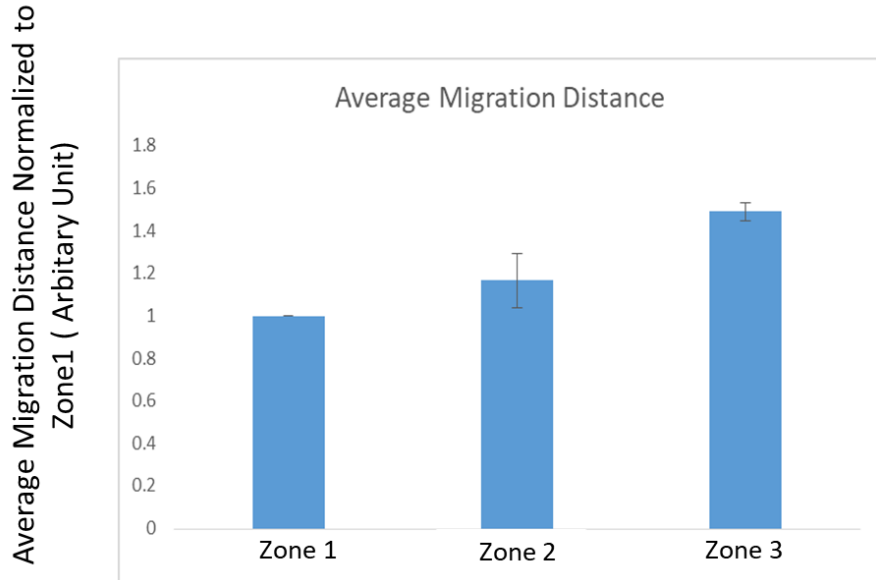
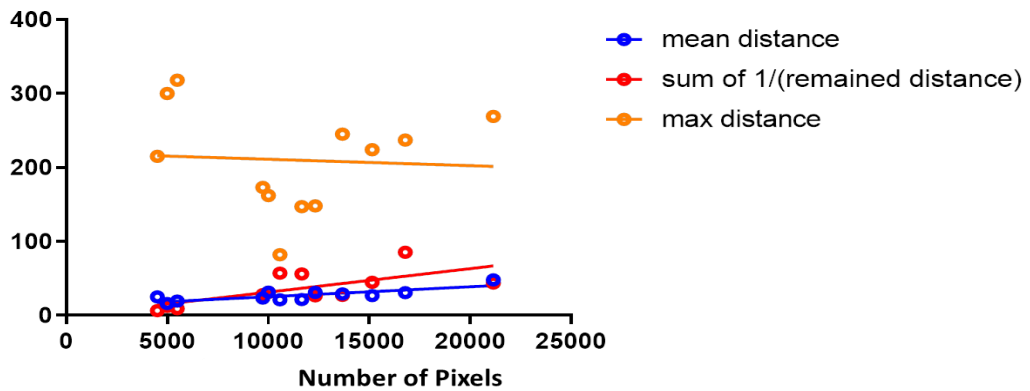


Figure 3.8. Average migrated distances for each region ANOVA  $p < 0.005$ .



	Significant?	R <sup>2</sup>	P value
Mean dist	Yes	0.64	0.0017
Sum of 1/dist	yes	0.47	0.0135
Max distance	ns	0	

Figure 3.9. Linear Regression Analysis for Mean Distance, Tension and Max Distance Anova  $p < 0.005$ .

Tension enforced to collagen gel and PDMS behind collagen is described as  $\Sigma(1/(\text{Remained distance to PDMS}))$  (Figure 3.8). Tension is investigated for each region, and 2<sup>nd</sup> and 3<sup>rd</sup> region normalized to 1<sup>st</sup> region (Figure 3.11). Significant difference was found between regions and tension was higher in zone 1.

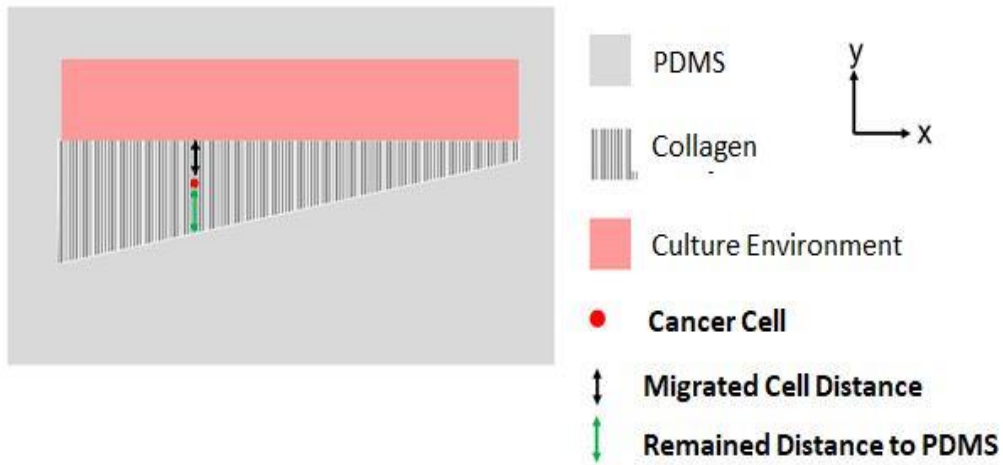


Figure 3.10. Illustration of migrated and remained distance.

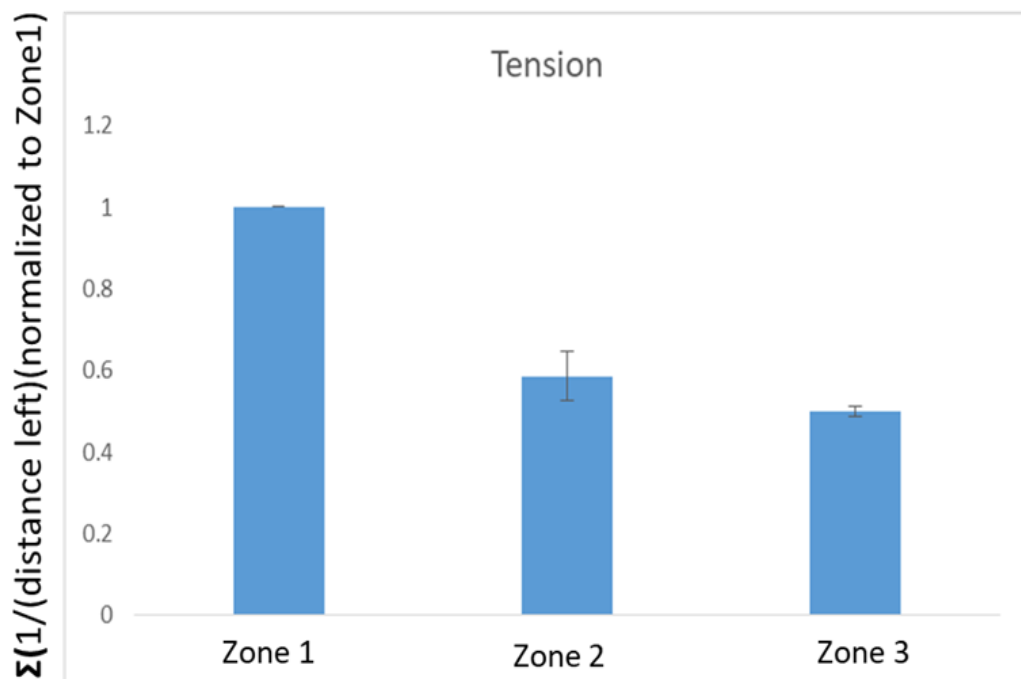


Figure 3.11. Tension for each zone, ANOVA  $p < 9.3 \times 10^{-6}$ .

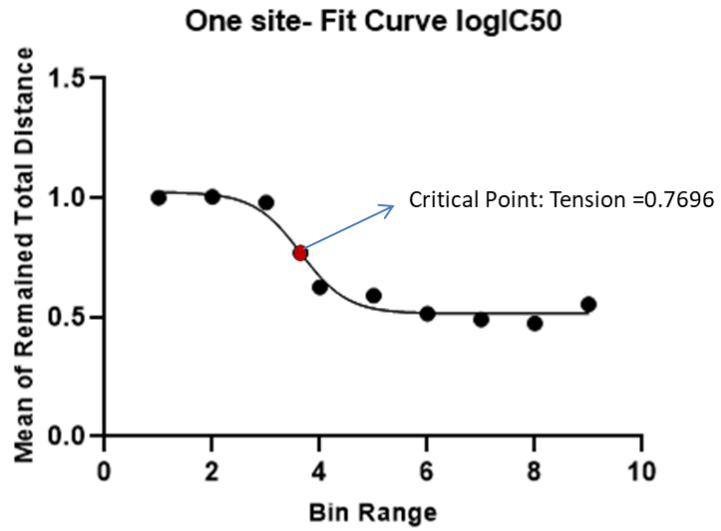


Figure 3.12. One site-Fit Curve logIC50 for tension.

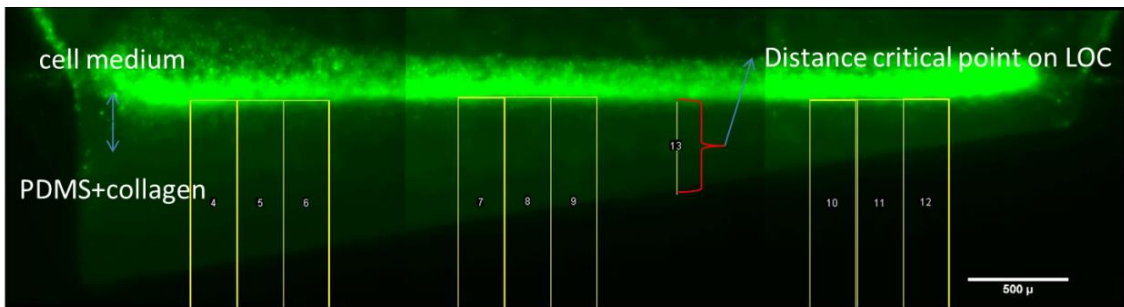


Figure 3.13. Critical Distance Point on LOC,  $450 \pm 7.1 \mu$ .

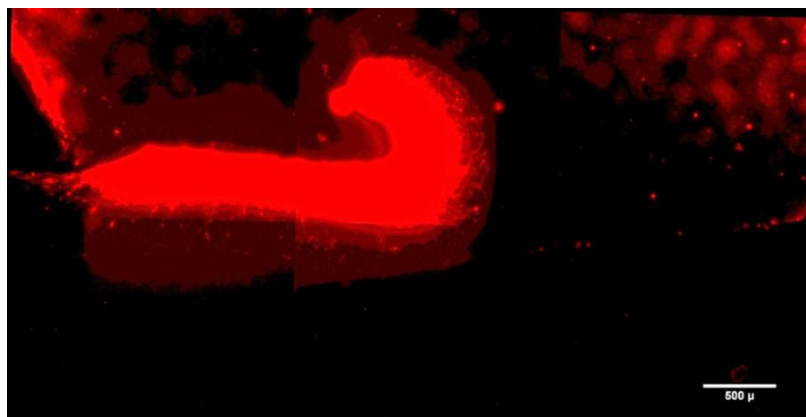


Figure 3.14. Collagen Detached from PDMS (After 6 days).

Table.1. Correlations between different parameters.

	Total Cellular Area	Total Migrated Distance	Average Migrated Distance	Tension
Total Cellular Area	1			
Total Migrated Distance	0.926415	1		
Average Migrated Distance	0.802346	0.938491	1	
Tension	0.687501	0.45878	0.276051	1

Correlation among total cellular area, total migrated distance, average migrated distance and tension parameters was investigated (Table 1). Although strong correlation was found between total cellular area and total/average migrated distance, weak correlation was found between tension and other parameters.

Then, as can be seen in figures, cellular migration was stopped in places where cells become close to PDMS surface. We investigated the cellular viability in each three region to see if the migration was stopped because cells died. The results obtained from PI/Hoechst double stain can be seen in Figure 3.15. As results show us, there is no relation between cellular death and proximity of cells to PDMS surface.

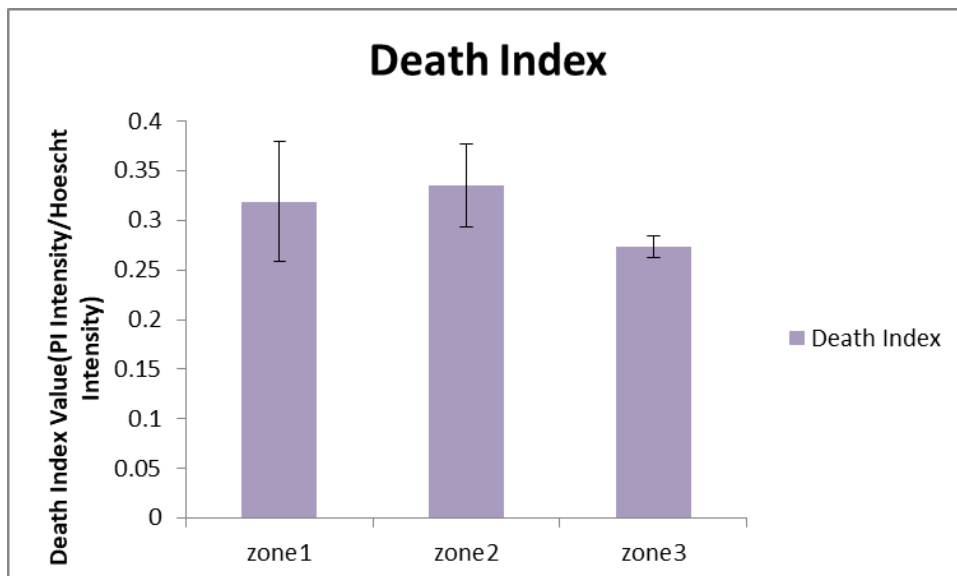


Figure 3.15. Death Index value (Viability) comparison among three zones, ANOVA  $p < 0.5978$ .

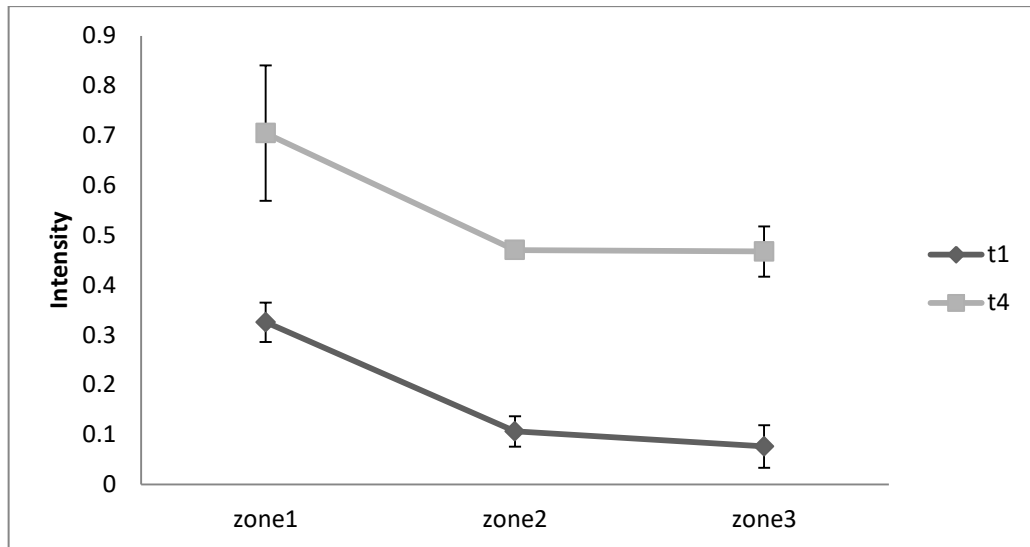


Figure 3.16. Permeability comparison among three zones, ANOVA  $p < 0.3988$  for t1 and ANOVA  $p < 0.1264$  for t4.

Additionally, collagen permeability was investigated to see the relation between cellular migration and collagen permeability. As we can hypothesize, cells migrated more in zone1 because the permeability of collagen was higher in zone1. However, the results show us there is no significant difference of collagen permeability among each zone (Figure 3.16).

## CHAPTER 4

### CONCLUSION

These results show cancer cells can sense stiffness at a distance in contrast to normal cells. If there was no mechanosensing at a distance, it is expected both of the cells to migrate same. The differences between migration distances support the idea of cellular mechanosensing at a distance in cancer cells. Cells couldn't reach to PDMS at the narrow site of it, in other words cellular migration is not limited with the area where cells can migrate. The expected result of decreasing cellular migration with distance was based on positive feedback, however obtained results shows stiffness at a distance leads to negative feedback. Cellular force by cancer cells can be transmitted to PDMS because of coated APTES chemistry of the LOC but also this force transmission is limited. After a point there will be no force transmission in LOC. This limit is longer than narrowest side (200micron) and shorter than the deepest region (1mm). Additionally, cells were cultured for twelve days to see the cellular migration limit and it was seen cells migrated maximum 350 micron. From these results it can be said there is biological limit for mechanosensing in cellular migration. Because the tension in first zone is higher, it illustrates that cells interact with PDMS better where they are close to it. And the tension in 2<sup>nd</sup> and 3<sup>rd</sup> zone is becoming small and these results sign interaction is decreasing when the distance between PDMS and cells decreases. In this case, maximum limit can be inside 2<sup>nd</sup> zone or at the end of 3<sup>rd</sup> zone where the average of collagen thickness is 447 micron. This value can be maximum limit for mechanosensing at a distance, but because cells migrated under this limit biologically it can be guessed that the limit can be at the end of 1<sup>st</sup> zone. For determination of the limit more accurately, calculations for obtained data can be done with computers that has high computing capability. Besides, new LOC designs can be developed that can enable chemotaxis and support mechanosensing.

Then, as can be seen in figures, cellular migration was stopped in places where cells become close to PDMS surface. We investigated the cellular viability in each three region to see if the migration was stopped because cells died. The results obtained

from PI/Hoechst double stain can be seen in Figure 3.13. As results show us, there is no relation between cellular death and proximity of cells to PDMS surface.

Additionally, collagen permeability was investigated to see the relation between cellular migration and collagen permeability. As we can hypnotize, cells migrated more in zone1 because the permeability of collagen was higher in zone1. However, the results show us there is no significant difference of collagen permeability among each zone (Figure 3.16).

It is difficult to say there is no mechanosensing at a distance in normal cells, because maybe they didn't migrate because they are not kind of intruder cells. Mechanosensing in these cells maybe couldn't be measured with this LOC system, so maybe mechanosensing in these cells happened in different way with these cells. For instance, cellular proliferation, differentiation in cell's cytoskeleton and etc. These points can be studied for future studies.

## REFERENCES

1. Tortora, G.J. and S.J.B.S.T.I. Grabowski, *Principles of anatomy and physiology*, 1996.
2. Manz, A., et al., *Planar chips technology for miniaturization of separation systems: a developing perspective in chemical monitoring*. 1993. **33**: p. 1-66.
3. Sonnen, K.F. and C.A.J.D.c. Merten, *Microfluidics as an emerging precision tool in developmental biology*. 2019. **48**(3): p. 293-311.
4. McDonald, J.C., et al., *Fabrication of microfluidic systems in poly (dimethylsiloxane)*. 2000. **21**(1): p. 27-40.
5. Bhattacharjee, N., et al., *The upcoming 3D-printing revolution in microfluidics*. 2016. **16**(10): p. 1720-1742.
6. Falconnet, D., et al., *Surface engineering approaches to micropattern surfaces for cell-based assays*. 2006. **27**(16): p. 3044-3063.
7. Whitesides, G.M., et al., *Soft lithography in biology and biochemistry*. 2001. **3**(1): p. 335-373.
8. Liotta, L.A., P.S. Steeg, and W.G.J.C. Stetler-Stevenson, *Cancer metastasis and angiogenesis: an imbalance of positive and negative regulation*. 1991. **64**(2): p. 327-336.
9. Jemal, A., et al., *Global cancer statistics*. 2011. **61**(2): p. 69-90.
10. Ferlay, J.J.I.c., *GLOBOCAN 2000. Cancer incidence, mortality and prevalence worldwide, version 1.0*. 2001.
11. Bray, F., P. McCarron, and D.M.J.B.c.r. Parkin, *The changing global patterns of female breast cancer incidence and mortality*. 2004. **6**(6): p. 229.
12. Theocharis, A.D., et al., *Extracellular matrix structure*. 2016. **97**: p. 4-27.
13. Shi, Q., et al., *Rapid disorganization of mechanically interacting systems of mammary acini*. 2014. **111**(2): p. 658-663.
14. Lu, P., V.M. Weaver, and Z.J.J.C.B. Werb, *The extracellular matrix: a dynamic niche in cancer progression*. 2012. **196**(4): p. 395-406.



15. Paszek, M.J., et al., *Tensional homeostasis and the malignant phenotype*. 2005. **8**(3): p. 241-254.
16. Kolahi, K.S., et al., *Effect of substrate stiffness on early mouse embryo development*. 2012. **7**(7): p. e41717.